CHEMISTRY
A EUROPEAN JOURNAL

DOI: 10.1002/chem.200700190

Synthesis and Characterization of Mononuclear Ruthenium(III) Pyridylamine Complexes and Mechanistic Insights into Their Catalytic Alkane Functionalization with *m*-Chloroperbenzoic Acid

Takahiko Kojima,*[a] Ken-ichi Hayashi,[a] Shin-ya Iizuka,[a] Fumito Tani,[b] Yoshinori Naruta,[b] Masaki Kawano,[c] Yuji Ohashi,[c] Yuichirou Hirai,[d] Kei Ohkubo,[d] Yoshihisa Matsuda,[a] and Shunichi Fukuzumi*[d]

Abstract: A series of mononuclear Ru^{III} complexes $[RuCl_2(L)]^+$, where L is tris(2-pyridylmethyl)amine (TPA) or one of four TPA derivatives as tetradentate ligand, were prepared and characterized by spectroscopic methods, X-ray crystallography, and electrochemical measurements. The geometry of a Ru^{III} complex having a non-threefold-symmetric TPA ligand bearing one dimethylnicotinamide moiety was determined to show that the nicotine moiety resides *trans* to a pyridine group, but not to the chlorido ligand. The substituents of the TPA ligands were shown to regulate the redox potential of the ruthenium center, as indicated by a linear Hammett plot in the range of 200 mV for Ru^{III}/Ru^{IV} couples with a relatively large ρ value (+0.150). These complexes act as effective catalysts for alkane functionalization in acetonitrile with *m*-chloroperbenzoic acid (*m*CPBA) as terminal oxidant at room temperature. They exhibited fairly good reactivity for oxidation of cyclohexane (C–H bond energy 94 kcal mol^{-1}), and the reactivity can be altered significantly by the electronic effects of substituents on TPA ligands in terms of initial rates and turnover numbers. Catalytic oxygenation of cyclohexane by a Ru^{III} complex with ^{16}O-*m*CPBA in the presence of $H_2{}^{18}O$ gave ^{18}O-labeled cyclohexanol with 100% inclusion of the ^{18}O atom from the water molecule. Resonance Raman spectra under catalytic conditions without the substrate indicate formation of a Ru^{IV}=O intermediate with lower bonding energy. Kinetic isotope effects (KIEs) in the oxidation of cyclohexane suggest that hydrogen abstraction is the rate-determining step and the KIE values depend on the substituents of the TPA ligands. Thus, the reaction mechanism of catalytic cyclohexane oxygenation depends on the electronic effects of the ligands.

Keywords: N ligands · oxygenation · reaction mechanisms · redox chemistry · ruthenium

Introduction

Developing highly effective and catalytic methods for functionalization of hydrocarbons, which are inert to chemical conversions, is one of the most important long-term tasks in chemistry and the chemical industry.[1] Such processes involve catalytic oxidation of hydrocarbons, especially alkanes as plentiful natural resources, and often require metal ions

[a] Dr. T. Kojima,[+] K. Hayashi, S. Iizuka, Prof. Dr. Y. Matsuda
Department of Chemistry
Faculty of Sciences
Kyushu University, Hakozaki
Higashi-Ku, Fukuoka 812-8581 (Japan)
E-mail: kojima@chem.eng.osaka-u.ac.jp

[b] Prof. Dr. F. Tani, Prof. Dr. Y. Naruta
Institute of Material Chemistry and Engineering
Kyushu University, Hakozaki, Higashi-Ku, Fukuoka 812-8581 (Japan)

[c] Prof. Dr. M. Kawano, Prof. Dr. Y. Ohashi
Department of Chemistry, Faculty of Science
Tokyo Institute of Technology
Ookayama, Meguro-Ku, Tokyo 152-8551 (Japan)

[d] Y. Hirai, Dr. K. Ohkubo, Prof. S. Fukuzumi
Department of Materials and Life Science
Graduate School of Engineering, Osaka University and SORST (JST)
2-1 Yamada-oka, Suita, Osaka 565-0871 (Japan)
Fax: (+81) 6-6879–7370
E-mail: fukuzumi@chem.eng.osaka-u.ac.jp

[+] Present address:
Department of Materials and Life Science
Graduate School of Engineering, Osaka University and SORST (JST)
2-1 Yamada-oka, Suita, Osaka 565-0871 (Japan)
Fax: (+81) 6-6879-7370

WILEY InterScience DISCOVER SOMETHING GREAT
© 2007 Wiley-VCH Verlag GmbH & Co. KGaA, Weinheim

as catalysts,[2] as observed in oxidations by metalloenzymes[3] and industrial cyclohexane oxidation for production of cyclohexanol and cyclohexanone on route to adipic acid.[4] As functional models of heme and non-heme iron enzymes, many catalytic systems based on Fe porphyrins[5] and Fe complexes with nitrogen-containing ligands[6] have been developed for oxidative functionalization of alkanes. The mechanisms of these catalytic oxidations have been reported to involve unstable and short-lived high-valent Fe^{IV} or Fe^{V} species as reactive intermediates.[7] Fe pyridylamine complexes, represented by Fe TPA complexes, have also been reported to perform catalytic hydroxylation of alkanes[8] and catalytic dihydroxylation of alkenes[9] with alkyl hydroperoxides and hydrogen peroxide. Que and co-workers have pointed out that the steric effects of 6-methyl groups in the TPA ligand play an important role in regulating the electronic character at the iron center.[10] However, changing the electronic effects of the TPA ligand by means of substituents has yet to be examined for tuning the reactivity at the metal center.

Besides the above Fe complexes, ruthenium complexes have been found to be effective in hydrocarbon functionalizations such as alkene epoxidation and alkane hydroxylation. A variety of ligands have been applied in these reaction systems, such as amine ligands[11] porphyrins,[12] phosphines,[13] and even polyoxometalates.[14] Among these, polypyridine ligands, represented by 2,2′-bipyridines and 1,10-phenanthrolines, have attracted much attention due to their robustness in the course of catalysis and accessibility to stable but reactive high-valent Ru=O complexes.[15] Pyridylamine ligands have yet to be utilized for the preparation of ruthenium-based catalyst systems for hydrocarbon oxidation. Che and co-workers reported that a ruthenium complex of tris(2-pyridylethyl)amine affords a Ru^{V}=O species which can oxidize alkanes.[16] They also demonstrated that ruthenium complexes of aliphatic amines perform catalytic hydrocarbon oxidations by using alkyl hydroperoxides.[17] Concerning ruthenium complexes of tris(2-pyridylmethyl)amine (TPA) and its derivatives, we and others have reported on their catalytic oxygenation of alkanes and proposed that the reactions proceed via formation of a high-valent Ru=O intermediates as reactive species.[18] Despite extensive efforts to confirm the formation of high-valent Ru=O intermediates, no direct information on such species has so far been reported.

Mechanistic investigations on alkane oxygenation by using metal complexes with peroxides always involve the question: What is the responsible species? The question is whether the reaction mechanism is metal-based, autoxidation by free radicals, or both. Usually, it is hard to elucidate the reaction mechanism. In general, the reaction mechanism has been simply assumed to be the same, and only substituent effects can be observed for catalysts having a series of ligands with the same scaffolds, for example, as reported for asymmetric epoxidation by manganese(III) salen complexes.[19]

We have reported the synthesis and characterization of ruthenium complexes of TPA derivatives[20] and their reactivity toward oxidative functionalization of hydrocarbons by using alkyl hydroperoxides[21] and molecular oxygen[22] in CH_3CN at room temperature. Here we describe the synthesis and characterization of a series of mononuclear Ru^{III} complexes of TPA derivatives to control the redox potential and elucidate the reaction mechanisms of alkane functionalization catalyzed by these complexes with *m*-chloroperbenzoic acid (*m*CPBA) as terminal oxidant. We demonstrate dramatic alteration of the reaction mechanism from radical-based autoxidation to a ruthenium oxo pathway by electronic effects of the TPA ligands. Regulation of the characteristics of the ruthenium oxo species is also reported.

Results and Discussion

Synthesis of Ru^{III} complexes: We synthesized a series of new TPA derivatives having substituents which can exert electronic effects on the metal center to control its reactivity. The synthesis of TPA derivatives with electron-donating groups did not raise serious problems, but that of TPAs with electron-withdrawing groups gave us serious problems, especially in their purification. We previously described synthetic procedures for Ru TPA complexes.[20a] However, the synthesis of mononuclear Ru^{III} complexes with TPA derivatives having electron-withdrawing substituents at the 5-position of the pyridine moiety gave lower yields of isolated products. We also tried to obtain Ru^{III} complexes with 5-COOR-TPA and 5-$(COOR)_2$-TPA (R = Me, Et), but these ligands decomposed during synthesis of Ru^{III} complexes. Therefore, to stabilize 5-substituted derivatives with electron-withdrawing groups, we prepared 5-$CONMe_2$-TPA, the amide moiety of which is more thermodynamically stable than ester groups. This strategy allowed us to obtain Ru TPA complex having electron-withdrawing groups at the 5-positions of pyridine rings of TPA such as $[RuCl_2\{5\text{-}(CONMe_2)\text{-}TPA\}]ClO_4$ and $[RuCl_2\{5\text{-}(CONMe_2)_2\text{-}TPA\}]ClO_4$. Like the 4-substituted TPA derivatives with electron-withdrawing ethoxycarbonyl (COOEt) groups, these ligands were stable under synthetic conditions and afforded mononuclear Ru^{III} complexes in good yields. The Ru^{III} complexes discussed in this paper are numbered as follows (Scheme 1): $[RuCl_2(TPA)]ClO_4$ (**1**), $[RuCl_2(5\text{-}Me_3\text{-}TPA)]ClO_4$ (**2**), $[RuCl_2\{5\text{-}(CONMe_2)\text{-}TPA\}]ClO_4$ (**3**), $[RuCl_2\{4\text{-}(COOEt)\text{-}TPA\}]ClO_4$ (**4**), and $[RuCl_2\{4\text{-}(COOEt)_2\text{-}TPA\}]ClO_4$ (**5**).

In the ^1H NMR spectrum of **1** in CD_3CN, signals were observed in the range from $\delta = -20$ to 40 ppm due to paramagnetic shift caused by the Ru^{III} ($S = 1/2$) center. A peak at 29.1 ppm is assigned to H5 of the pyridine rings due to the absence of such a peak in the spectrum of **2**. Thus, the ^1H–^1H COSY spectrum of **1** in Figure 1 allows us to assign the paramagnetically shifted peaks. A peak at $\delta = 38.8$ ppm shows no cross-peaks and is easily assigned to the methylene protons, and this should be due to dipole–dipole contact shift. Resonances at $\delta = 11.3$ and 18.7 ppm are attributed to

 © 2007 Wiley-VCH Verlag GmbH & Co. KGaA, Weinheim

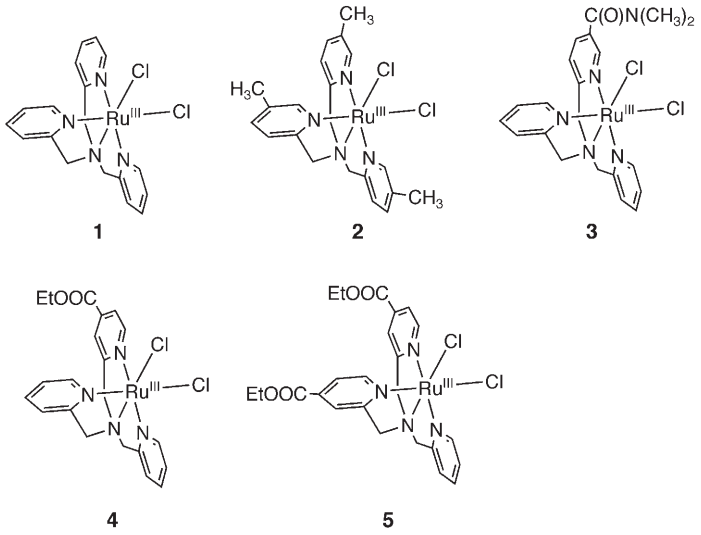

Scheme 1. Mononuclear Ru^{III} complex cations discussed in this paper.

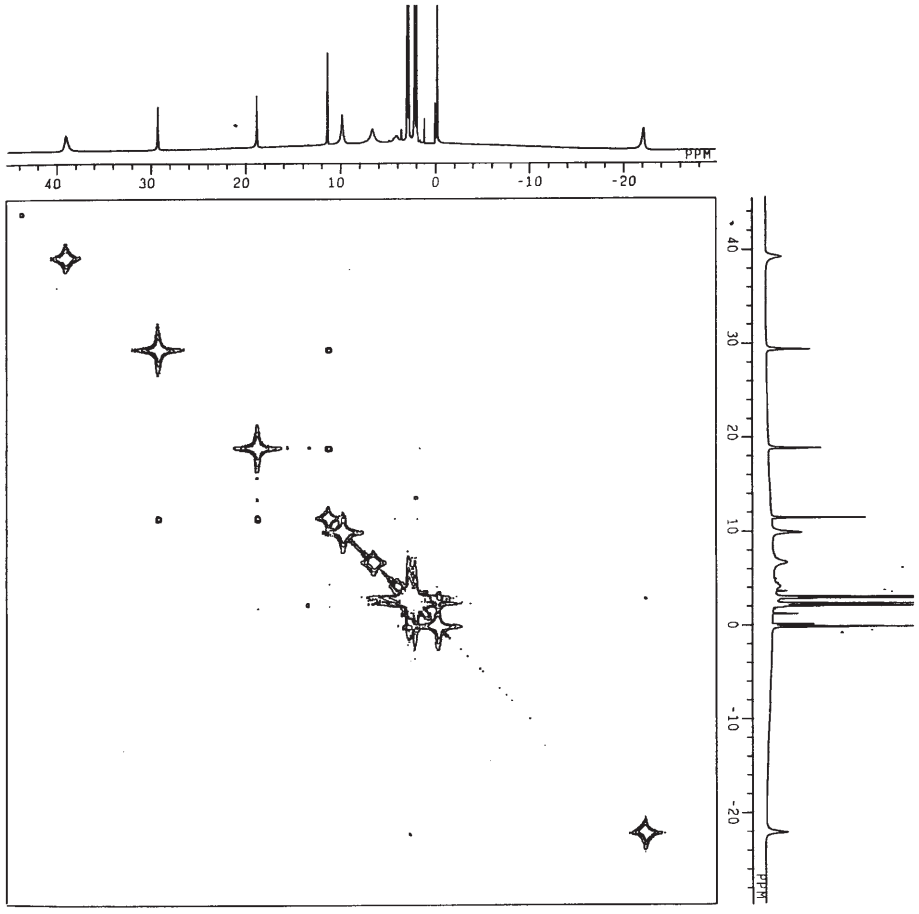

Figure 1. ^1H–^1H COSY spectrum of **1** in CD_3CN at room temperature.

pyridine H4 and H3, respectively. The most upfield-shifted signal at $\delta = -22.1$ ppm is assigned to pyridine H6. Resonances at $\delta = -0.2$, 2.9, 6.5, and 9.7 ppm are probably due to one nonequivalent pyridine ring. These results suggest that the unpaired electron in the dπ orbital of the Ru^{III} center interacts with π* orbitals of the two equivalent pyridine rings through dπ–pπ* interaction, and this causes alternative shifts in the signals of the pyridine protons.

Molecular structures of $[RuCl_2(5\text{-}Me_3\text{-}TPA)]PF_6$ (2′) and $[RuCl_2(5\text{-}CONMe_2\text{-}TPA)]ClO_4 \cdot {}^1/_2\,C_2H_5OH$ ($3 \cdot {}^1/_2\,C_2H_5OH$): Complex **2′** crystallized in the monoclinic space group $P2_1/a$ without solvent molecules of crystallization. An ORTEP drawing is depicted in Figure 2, and selected bond lengths and angles are listed in Table 1. The geometry around the ruthenium center of **2** is nearly identical to that of **1** except for the Ru–Cl bond lengths: Those of **2′** were determined to be 2.358(1) Å for that *trans* to the tertiary amino group and 2.3316(6) Å for that *trans* to a pyridine moiety, while the corresponding bond lengths in **1** are 2.330(2) and 2.357(2) Å, respectively.[20a]

Complex **3** has two possible geometries: A substituted pyridine moiety coordinates to the position *trans* to symmetrical monosubstituted TPA derivatives or *trans* to chloride. We determined the crystal structure of $[RuCl_2(5\text{-}CONMe_2\text{-}TPA)]ClO_4$. A single crystal suitable for X-ray crystallography was obtained by recrystallization from a solution of **3** in CH_2Cl_2/EtOH. The X-ray analysis revealed the geometry of **3** shown in Figure 3.

Selected bond lengths and angles are listed in Table 2. As shown in Figure 3, the 5-$CONMe_2$-pyridine ring (dimethylnicotinamide) is located in a position *trans* to an unsubstituted pyridine ring, rather than *trans* to Cl^-. Interestingly, the Ru–N2 and Ru–N4 bond lengths are the same (2.063(4) Å) and shorter than those of **1** (2.074(5) and 2.073(5) Å), while the Ru–N3 is similar to that of **1**.[20a] The dimethylamide moiety is planar and displaced from the pyridyl plane with a torsion angle of −41.8°. The crystal structure of $\{Cd(NCS)(N,N\text{-diethylnicotinamide})_2\}_n$ revealed similar disposition of the amide moiety.[23] Karlin and co-workers have also reported on the synthesis and characterization of a Cu^I complex of a TPA derivative having a 5-methoxycarbonyl group on a pyridine ring. This complex also exhibited no significant differences among the Cu–N(py) bond lengths.[24] One example

 © 2007 Wiley-VCH Verlag GmbH & Co. KGaA, Weinheim

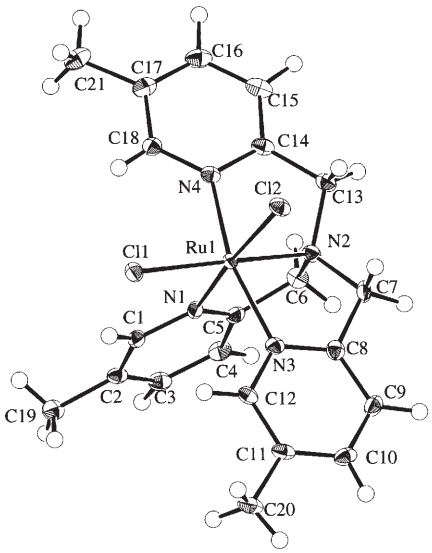

Figure 2. ORTEP drawing of the cation of **2′** with numbering scheme. Thermal ellipsoids are drawn at 50% probability.

Table 1. Selected bond lengths [Å] and angles [°] for **2′**.

Ru1−Cl1	2.358(1)	Ru1−Cl2	2.3316(6)
Ru1−N1	2.073(2)	Ru1−N2	2.070(3)
Ru1−N3	2.072(2)	Ru1−N4	2.056(3)
Cl1-Ru1-Cl2	91.31(3)	Cl1-Ru1-N2	176.01(7)
Cl2-Ru1-N1	174.43(10)	N2-Ru1-N1	82.0(1)
N2-Ru1-N3	82.5(1)	N2-Ru1-N4	80.5(1)
N3-Ru1-N4	163.0(1)		

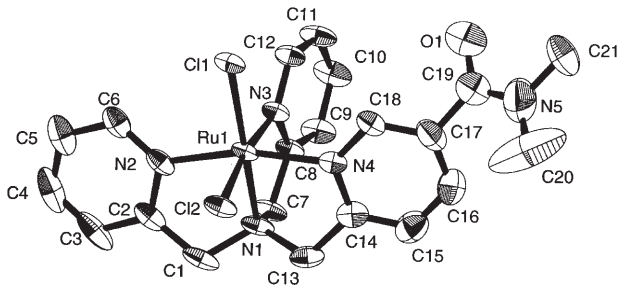

Figure 3. ORTEP representation of the cation of **3** with numbering scheme. Thermal ellipsoids are drawn at 50% probability level.

Table 2. Selected bond lengths [Å] and angles [°] for **3**·C_2H_5OH.

Ru1−Cl1	2.345(1)	Ru1−Cl2	2.346(1)
Ru1−N1	2.068(4)	Ru1−N2	2.063(4)
Ru1−N3	2.083(4)	Ru1−N4	2.063(5)
O1−C19	1.271(11)	N5−C19	1.359(13)
N5−C20	1.54(2)	N5−C21	1.444(11)
C17−C19	1.466(10)		
Cl1-Ru1-Cl2	93.48(3)	N1-Ru1-N2	81.3(2)
N1-Ru1-N3	82.1(2)	N1-Ru1-N4	82.7(2)
Cl1-Ru1-N1	174.7(1)	Cl2-Ru1-N3	171.9(1)
N2-Ru1-N4	164.0(2)	O1-C19-C17	120.4(9)
O1-C19-N5	121.3(9)	C19-N5-C20	127.8(11)
C19-N5-C21	117.2(10)	C20-N5-C2	113.9(12)

of coordination of nicotinamide to a ruthenium ion has been reported, albeit without X-ray analysis; the Ru^{II} or Ru^{III} ion is coordinated by four nicotinamides which are bound to *meso*-phenyl groups of a tetraphenylporphine derivative.[25]

Electrochemical measurements on Ru^{III} TPA complexes: To assess the electronic effects of substituents on the pyridine ring(s) of TPA ligands on the electron density at the ruthenium center, cyclic voltammetry was performed on the mononuclear Ru^{III} complexes **1**–**5** in CH_3CN in the presence of 0.1 M nBu$_4$NClO$_4$ under N_2 at ambient temperature. The complexes exhibited two reversible redox waves assignable to Ru^{II}/Ru^{III} and Ru^{III}/Ru^{IV} couples. The potentials were determined relative to ferrocene/ferricenium couple at 0 V and are listed in Table 3. The redox potentials can be varied

Table 3. Redox potentials [V] of mononuclear Ru^{III} complexes and kinetic isotope effects (KIE) in cyclohexane hydroxylation.

Complex	$\Sigma\sigma$[a]	Ru^{II}/Ru^{III}[b]	Ru^{III}/Ru^{IV}[b]	KIE[c]
2	−0.207	−0.26[b]	1.34[b]	3.9
1	0	−0.23[b]	1.37[b]	3.1
3	0.280	−0.19	1.41	5.7
4	0.522	−0.16	1.44	3.7
5	1.044	−0.05	1.53	4.3

[a] From ref. [26]. [b] Potentials were measured by cyclic voltammetry in CH_3CN in the presence of 0.1 M nBu$_4$NClO$_4$ as supporting electrolyte under N_2 at room temperature. The values were determined relative to the ferrocene/ferricenium redox couple (0 V). [c] Cyclohexane/[D_{12}]cyclohexane (1/1) as substrate; values for cyclohexanol formation.

over a wide range up to 1.53 V relative to ferrocene/ferricenium couple. A Hammett plot of the Ru^{III}/Ru^{IV} redox potentials showed a linear relationship (Figure 4),[26] which indicates that the electron density at the ruthenium center is governed by substituents on the pyridine rings. Based on this linear relationship, we can predict redox potentials of $[RuCl_2(TPA\ derivative)]^+$ complexes yet to be synthesized. This kind of behavior has been observed in hydroxo Fe^{III} porphyrin complexes[27,28] and Mn^{III} salen complexes.[29] The ρ value of +0.150 is much larger than that of +0.075 observed for Fe^{III} porphyrins in which the substituents are located on phenyl groups at meso positions of tetraphenylporphyrin derivatives. This comparison suggests that the substituents on the pyridine rings of TPA can exert larger electronic effects on reactivity at the metal center. The ρ value of +0.150 of the Ru TPA complexes is comparable to that of the Ru bpy complexes (ρ = +0.175 for $\Sigma\sigma$).[30] The relationship between the redox potentials of Ru^{II}/Ru^{III} and Ru^{III}/Ru^{IV} couples is shown in Figure 4b, and the linear relationship indicates that the structural change is very small. This indicates that very small reorganization energies are required in the course of the redox processes.

Electrochemical oxidation of Ru^{III} TPA complexes afforded Ru^{IV} TPA complexes. Bulk electrolysis of **1**–**5** in CH_3CN at 298 K in the presence of 0.1 M TBAP gave reversible spectral changes in their UV/Vis spectra. The spectral change on oxidation were minor, as shown in Figure 5: the absorption

 © 2007 Wiley-VCH Verlag GmbH & Co. KGaA, Weinheim

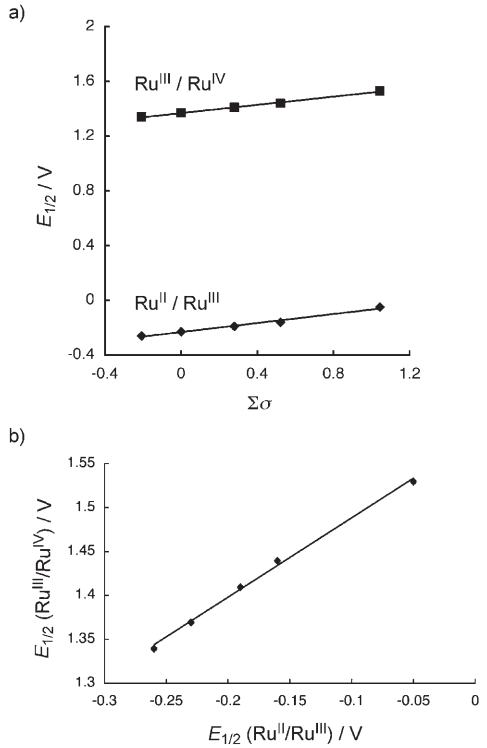

Figure 4. Hammett plot for the redox potentials of Ru^{II}/Ru^{III} and Ru^{III}/Ru^{IV} couples in CH_3CN (0.1 M TBAP) at room temperature (a) and relationship between potentials of Ru^{II}/Ru^{III} couples and Ru^{III}/Ru^{IV} couples (b).

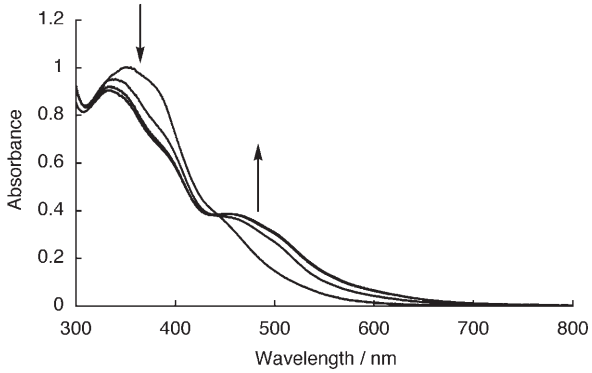

Figure 5. Spectral changes in the course of electrochemical oxidation of **5** at 2.00 V (vs. SCE) in CH_3CN in the presence of 0.1 M TBAP at room temperature.

maximum at 424 nm shifted to 435 nm and slightly increased in intensity, whereby the color changed from orange to reddish orange. In contrast to oxidation, reduction led to dramatic spectral changes in each case: A new intense absorption band appeared at 370–550 nm during electrochemical reduction at −0.10 V (vs. SCE), as shown in Figure 6 for the case of **1**. The absorption maxima of Ru^{II} complexes generated by electrochemical reduction of **1**–**5** are summarized in Table 4.

Electronic effects on catalytic oxygenation of cyclohexane by 1–5 with *m*-chloroperbenzoic acid in CH_3CN: We exam-

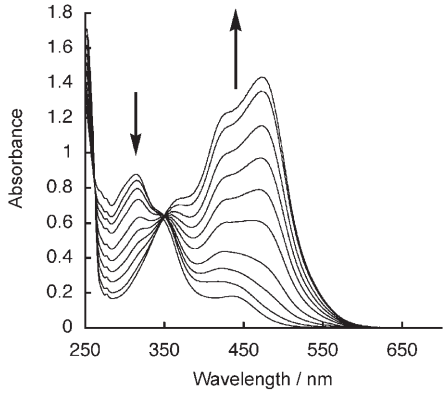

Figure 6. Spectral changes in the course of electrochemical reduction of **1** at −0.10 V (vs. SCE) in CH_3CN in the presence of 0.1 M TBAP at room temperature.

Table 4. Absorption maxima of UV/Vis spectra of reduced species for **1**–**5** in CH_3CN at room temperature.[a]

Complex	λ_{max} [nm]
1	473
2	472
3	480, 429
4	542, 432
5	553, 475

[a] Reduction was performed at −0.1 V (vs SCE) in the presence of 0.1 M TBAP.

ined the catalytic oxidation of cyclohexane by the Ru^{III} TPA complexes with *m*CPBA as terminal oxidant in CH_3CN at room temperature and monitored the reactions by GC analysis. Under these conditions, no oxidation products of cyclohexane were observed in the absence of catalyst.

Each complex exhibited catalytic activity toward oxygenation of cyclohexane to give cyclohexanol (CyOH), cyclohexanone (CyO), and small amount of chlorocyclohexane (CyCl). The formation of CyCl should be independent of the catalysts and originate from a radical process involving formation of $Cl^{\bullet}$ by reaction of Cl^- with *m*CPBA, as reported previously.[31] We focus on the reactions of **1** with unsubstituted TPA and **5** with TPA bearing electron-withdrawing groups at the 4-position of two pyridine moieties. We observed substituent effects on the rate of catalytic oxygenation in the initial stage and differences in the amount of products including CyOH, CyO, and CyCl.

The time course of product formation is shown in Figure 7 for the case of **1** as catalyst. Production of CyOH and CyO exhibited induction periods and both products were formed at comparable rates, whereas PhCl was formed without an induction period. The simultaneous formation of CyOH and CyO indicates that they are mainly formed via the bimolecular disproportionation of cyclohexylperoxyl radicals in the autoxidation of cyclohexane (a radical chain process; see below).[32]

In sharp contrast to **1**, the reaction catalyzed by **5** proceeds efficiently with a totally different time-course profile (Figure 8). In this case, CyOH is formed prior to formation of CyO, and the decrease in CyOH production is accompa-

 © 2007 Wiley-VCH Verlag GmbH & Co. KGaA, Weinheim

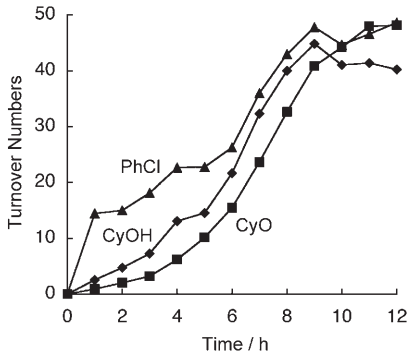

Figure 7. Time course of formation of CyOH, CyO, and PhCl in the **1**-catalyzed oxidation of cyclohexane (1.9 M) with *m*CPBA (200 mM) in CH_3CN (5 mL) at room temperature; [**1**] = 2 mM.

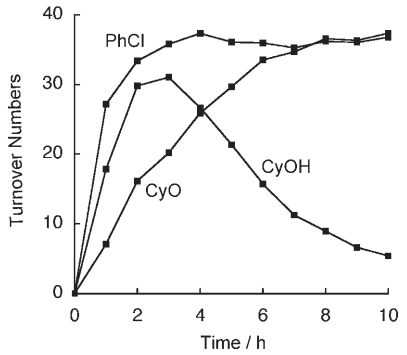

Figure 8. Time course of formation of CyOH, CyO, and PhCl in the **5**-catalyzed oxidation of cyclohexane (1.9 M) with *m*CPBA (200 mM) in CH_3CN (5 mL) at room temperature; [**5**] = 2 mM.

nied by an increase in CyO. This clearly indicates that CyO is produced by further oxidation of CyOH and that autoxidation is not the major pathway in the catalytic oxygenation of cyclohexane with **5**. It was confirmed that the oxidation of CyOH afforded CyO as sole product under the same conditions with a turnover number of 82 over 1 h.[33] The amount of PhCl formed in the reaction of **5** with *m*CPBA was also determined as 7 equiv of **5** by GC in the absence of the substrate. We also confirmed the formation of *m*CBA by NMR spectroscopy. Based on mass balance, Baeyer–Villiger reaction of CyO to form caprolactone was not detected in our GC-MS analysis.

We determined kinetic isotope effects ($KIE = k_H/k_D$) for cyclohexane oxygenation by **1**–**5** and *m*CPBA with a 1:1 mixture of cyclohexane and [D_{12}]cyclohexane as substrate in CH_3CN under the same conditions (Table 3). We determined an appropriate reaction time for each catalyst based on its time course of product formation (see above). Chlorination of cyclohexane can be performed by *m*CPBA in the presence of chloride ion, and the KIE values (5.6–6.3) are consistent with these radical reactions.[31] In contrast, the KIE values for hydroxylation exhibited a larger range of 3.1–5.7.

The KIE values for CyOH formation by **1** and **5** were determined to be 3.1 and 4.3, respectively. These values are as low as those of reactions in which hydrogen abstraction is performed by free radicals. These observations indicate that the species responsible for hydrogen abstraction should have a strong radical character.[34] As can be seen in Figures 7 and 8, the reactive species in the reactions with **1** and **5** should be totally different.

Mechanistic insights into catalytic cyclohexane hydroxylation: To gain mechanistic insights into cyclohexane oxygenation, labeling experiments were performed in the presence of $H_2{}^{18}O$ under the same experimental conditions, and the products were analyzed by GC-MS to examine the incorporation of ^{18}O from $H_2{}^{18}O$ into CyOH.[35] In the case of **1**, only 9% of ^{18}O was incorporated into CyOH. In contrast, the catalytic production of CyOH with **5** exhibited 100% ^{18}O incorporation. This type of incorporation has been reported by Nam and co-workers to be diagnostic of the existence of a high-valent metal oxo species that is responsible for hydroxylation.[36] This indicates that the reaction of **5** with *m*CPBA affords a high-valent Ru=O species which is responsible for cyclohexane hydroxylation, whereas that of **1** gives free-radical species derived from *m*CPBA and leads to autoxidation of cyclohexane.

First, we consider the reaction mechanism of oxygenation with **1**. The initiation of the radical-chain process should occur by the Haber–Weiss mechanism involving electron transfer from *m*CPBA to the Ru^{III} center to form Ru^{II} species and an acylperoxyl radical (*m*CPB$^{\bullet}$) that undergoes a bimolecular reaction to produce *m*-chlorobenzoyl radical (*m*CPB$^{\bullet}$), and also electron transfer from the Ru^{II} center to *m*CPBA to form Ru^{III} species and the carboxyl radical (*m*CBA$^{\bullet}$) (Scheme 2). The *m*CBA$^{\bullet}$ radical is known to be readily decarboxylated to produce the highly reactive *m*-chlorophenyl radical.[37] Thus, we propose the oxidation mechanism of cyclohexane by **1** with *m*CPBA in Scheme 3. *m*-Chlorophenyl radical produced by the reaction of *m*CPBA and **1** (Scheme 2) abstracts a hydrogen atom from

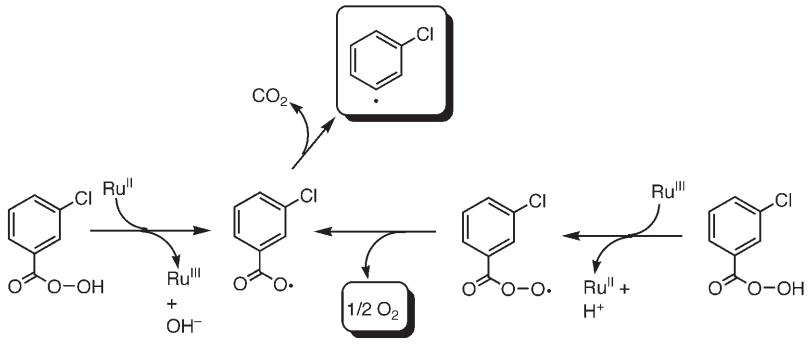

Scheme 2. Ruthenium-catalyzed decomposition of *m*CPBA to form radical species.

© 2007 Wiley-VCH Verlag GmbH & Co. KGaA, Weinheim

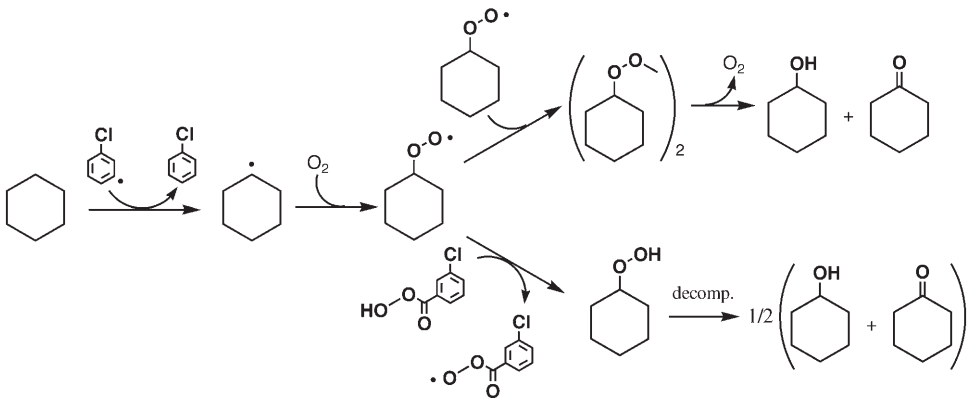

Scheme 3. Proposed mechanism of formation of CyOH and CyO in autoxidation.

cyclohexane to afford a cyclohexyl radical (Scheme 3). The phenyl C–H bond energy has been reported to be 104 kcal mol^{-1};[38] therefore, it is possible to abstract hydrogen from cyclohexane with a C–H bond energy of 94 kcal mol^{-1}.[38] Minisci and co-workers claimed that the hydrogen abstraction can be performed by *m*CPB$^{\bullet}$ in adamantane oxidation;[39] however, the ArC(O)OO–H bond energy is known to be about 90 kcal mol^{-1}, which should be enough to abstract hydrogen from the tertiary C–H bonds of adamantane but not sufficient for the C–H bonds of cyclohexane.

Another candidate for the hydrogen-abstracting species in cyclohexane oxygenation is *m*CBA$^{\bullet}$; the bond energy of ArC(O)O–H has been reported to be greater than 100 kcal mol^{-1}. In our case, since a comparable amount of PhCl can be obtained, we can rule out participation of *m*CBA$^{\bullet}$ as a major hydrogen-abstracting species. Thus, the species responsible for hydrogen abstraction in cyclohexane oxygenation is chlorophenyl radical, rather than *m*CBA$^{\bullet}$, as shown in Scheme 3. The cyclohexyl radical can react with O_2 to give cyclohexylperoxyl radical, which undergoes a well-known bimolecular disproportionation to give CyOH and CyO, accompanied by O_2 evolution, or abstracts a hydrogen atom from *m*CPBA to form cyclohexyl hydroperoxide, which decomposes to CyOH and CyO. The *m*CPB$^{\bullet}$ radical produced in the hydrogen-abstraction reaction undergoes a bimolecular reaction to produce *m*CBA$^{\bullet}$, which is readily decarboxylated to produce chlorophenyl radical (Scheme 3). Thus, once chlorophenyl radical is produced by reaction of *m*CPBA with **1** (Scheme 2), it acts as a radical chain carrier in the radical chain oxygenation of cyclohexane (Scheme 3). This mechanism is consistent with the observation that CyOH and CyO are concomitantly obtained with comparable rates and amounts (Figure 7).

Catalytic hydroxylation by **5** is in sharp contrast to that by **1** in terms of time course of product formation, KIE value, and the incorporation of ^{18}O from $H_2{}^{18}O$ into CyOH (see above). In the course of the reaction of **5** with *m*CPBA in CH_3CN, we could observe spectral changes of the solution at −30 °C: absorption increased around 400 nm and decreased in the range of 500–600 nm (Figure 9). The spectral change is different from that in the electrochemical oxidation of **5** to form the Ru^{IV} complex $[Ru^{IV}Cl_2\{(4\text{-}COOEt)_2\text{-}TPA\}]^{2+}$ (Figure 5). In this case, a Ru^{IV}=O complex is a putative candidate for the reactive intermediate in the catalytic oxygenation of cyclohexane.

To obtain direct evidence to support formation of a high-valent Ru=O intermediate in the **5**/*m*CPBA system, we recorded Raman spectra (excitation at 413.1 nm) on the reaction mixture of **5** and *m*CPBA in CH_3CN under the catalytic conditions in the presence of $H_2{}^{16}O$ or $H_2{}^{18}O$ at −30 °C. In the case of $H_2{}^{16}O$, a resonance was observed at 752 cm^{-1}, which completely shifted to 708 cm^{-1}, when $H_2{}^{16}O$ was replaced by $H_2{}^{18}O$ (Figure 10).

The Ru=O stretching frequencies have been reported to be 818 cm^{-1} for $[\{Ru^{IV}(O)(bpy)_2\}_2O]^{4+}$,[40] 780 cm^{-1} for $[Ru^{IV}(O)(tpp)]$ (tpp = tetraphenylporphinato),[41] and

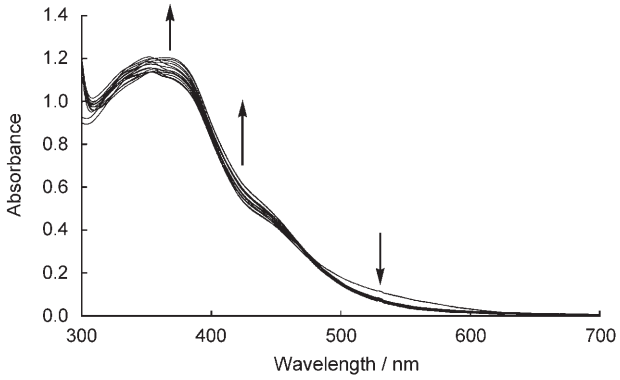

Figure 9. UV/Vis spectral changes in the course of the reaction of **5** (0.13 mM) with *m*CPBA (50 equiv, 6.5 mM) in CH_3CN at −30 °C.

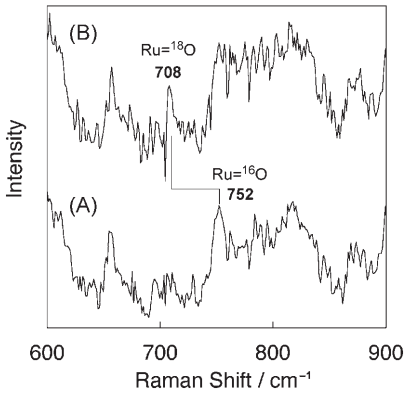

Figure 10. Resonance Raman spectra of reaction mixtures of **5** and *m*CPBA (30 equiv) in the presence of $H_2{}^{16}O$ (A) and $H_2{}^{18}O$ (B) in CH_3CN at −30 °C.

 © 2007 Wiley-VCH Verlag GmbH & Co. KGaA, Weinheim

872 cm^{-1} (IR) for a Ru^{V}=O complex.[16] Comparison of the observed value to those reported for Ru=O species strongly suggests that the intermediate derived from the reaction of **5** with *m*CPBA is a Ru^{IV}=O species. The relatively weak Ru=O bond, indicated by the low Ru=O stretching frequency compared to other Ru^{IV}=O complexes, may facilitate rapid exchange of oxygen with water prior to hydrogen abstraction ($k_H/k_D = 4.3$) to give ^{18}O-labeled CyOH selectively (vide supra).

In the case of the reaction of **1** with *m*CPBA in CH_3CN, we could not observe a signal assignable to the stretching vibration of a Ru^{IV}=O moiety in the resonance Raman spectrum. This is probably due to not only its small quantity based on 9% incorporation of ^{18}O from $H_2{}^{18}O$ into cyclohexanol but also to overlap of the peak with other, strong signals.

A proposed reaction mechanism for the catalytic cycle involving **5** that includes formation of the Ru^{IV}=O intermediate is shown in Scheme 4. Reaction of **5** with *m*CPBA affords Ru acylperoxo complex **A**, in which O–O bond homolysis occurs to produce a Ru^{IV}=O species and the carboxyl radical. The Ru^{IV}=O species can oxygenate cyclohexane to yield CyOH, which is further oxidized to CyO, accompanied by formation of the Ru^{II} complex. Ruthenium acylperoxo complex **A** is regenerated by reaction of the Ru^{II} complex with the acylperoxyl radical, which is produced by hydrogen abstraction from *m*CPBA by the decarboxylated radical,[42] accompanied by formation of PhCl. Formation of a Ru^{IV}=O species is dominant when a catalyst with an electron-deficient metal center, as in **5**, is used to conduct the hydroxylation of cyclohexane, due to the higher redox potential compared to **1**. The lower redox potential of catalyst **1** facilitates outer-sphere electron transfer to generate radical species for radical-chain reactions based on the Ru^{II}/Ru^{III} redox process.[20a] In contrast, the higher redox potential of catalyst **5** makes electron transfer energetically difficult when a Ru^{IV}=O species is generated via acylperoxo intermediate **A**. The higher redox potential of the ruthenium center in **5** suppresses electron transfer to form free-radical species for radical autoxidation, and enhances the formation and reactivity of the Ru^{IV}=O species toward hydrogen abstraction from the strong C–H bonds of cyclohexane. Thus, changing the electronic effect of the TPA ligand drastically alters the reaction mechanism of the oxygenation of cyclohexane from the autoxidation pathway in the case of **1** to the catalytic hydroxylation of cyclohexane via formation of a Ru^{IV}=O species in the case of **5**.

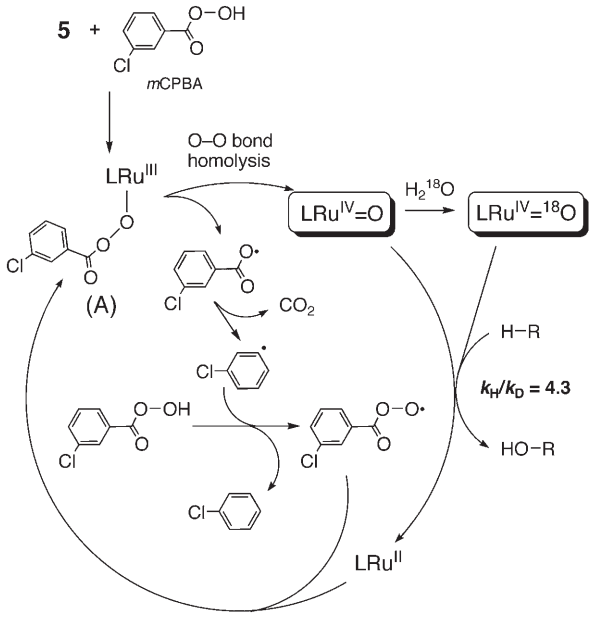

Scheme 4. Proposed reaction mechanism of catalytic hydroxylation of cyclohexane by *m*CPBA and **5**.

The reactivity of the Ru^{IV}=O species derived from **5** is high enough to abstract hydrogen from cyclohexane with a KIE value of 4.3. This high reactivity can be ascribed to radical character of the Ru^{IV}=O species. In this case, the high potential of the ruthenium center favors the Ru^{III} oxidation state, and the electron density at the oxygen atom would be pulled back to the ruthenium center to increase the radical character of the oxygen atom (Scheme 5). This pronounced radical character would enable hydrogen abstraction from cyclohexane and lead to lower Ru=O bond energy, as observed in its Raman spectrum (Figure 10), which facilitates ^{18}O exchange with $H_2{}^{18}O$. Jitsukawa and co-workers have also claimed radical character of RuO species derived from Ru TPA complexes based on product analysis.[43]

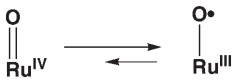

Scheme 5. Radical character of the Ru^{IV}=O species derived from **5**.

Conclusion

We have synthesized a series of mononuclear Ru^{III} complexes of TPA derivatives to control the redox potential of the ruthenium center. The redox potentials can be regulated in accordance with the electronic effects of substituents on the TPA ligands. The reaction mechanism of catalytic alkane oxygenation by these complexes with *m*CPBA was altered by the electronic characteristics at the ruthenium center. We have also succeeded in detecting a reactive Ru^{IV}=O intermediate derived from a mononuclear Ru^{III} TPA complex with electron-withdrawing groups (COOEt), which acts as an effective catalyst for the oxygenation of cyclohexane. Formation of the Ru^{IV}=O intermediate in the catalytic oxygenation reaction was confirmed by 100% ^{18}O incorporation from $H_2{}^{18}O$ into the alcohol product and detection of a signal due to ν(Ru=O) at 752 cm^{-1} in the Raman spectrum, which is lower than those of Ru^{IV}=O complexes reported so far. This high reactivity, the feasibility of isotopic exchange, and the lower energy of Ru=O stretching are consistent with Ru^{III}–$O^{\bullet}$ character of the Ru^{IV}=O intermediate.

 © 2007 Wiley-VCH Verlag GmbH & Co. KGaA, Weinheim

Experimental Section

General: CH_3CN was distilled from CaH_2 under N_2 and stored over 4 Å molecular sieves. $CHCl_3$ was distilled from CaH_2 under N_2 immediately prior to use. *m*CPBA was purified by a literature method. All other solvents were of special grade and were used as received from commercial sources without further purification. Analytical thin-layer chromatography was performed on silica gel Merck 60 F_{254} or alumina 60 F_{254} aluminum-backed plates. Column chromatography was performed on silica gel Waco-gel C-200 (60–200 mesh) or activated alumina (ca. 200 mesh), both from Waco pure chemicals. ^{1}H NMR and ^{1}H–^{1}H COSY spectra were recorded on JEOL EX-270 (270 MHz) or JEOL GX-400 (400 MHz) spectrometers. UV/Vis absorption spectra were recorded on a Jasco Ubest-55 UV/Vis spectrophotometer at room temperature. FAB-MS spectra were obtained on a JEOL JMS-SX/SX102A Tandem Mass spectrometer. Elemental analysis was performed at the Service Center of the Elemental Analysis of Organic Compounds, Department of Chemistry, Kyushu University. IR spectra were measured on a Jasco IR model 800 infrared spectrophotometer in the range of 400–4000 cm^{-1}. Gas chromatography was performed on a Shimadzu GC-14B instrument.

Synthesis: TPA·3$HClO_4$[44] and 5-Me_3-TPA[45] were prepared by literature methods.

5-Ethoxycarbonyl-2-chloromethylpyridine hydrochloride: $SOCl_2$ (12.3 g, 0.10 mol) in $CHCl_3$ (50 mL) was added dropwise to an ice-cooled solution of 5-methoxycarbonyl-2-hydroxymethylpyridine (2.68 g, 14.8 mmol) in $CHCl_3$ under N_2. The solution was stirred overnight at room temperature. $CHCl_3$ and excess $SOCl_2$ were removed to give a reddish white solid. This material was used for further synthesis without any purification. ^{1}H NMR ($CDCl_3$): $\delta = 9.26$ (d, 2 Hz, 1H, H6), 8.96 (dd, 1H, $J = 8$, 2 Hz, H4), 8.21 (d, 1H, $J = 8$ Hz, H3), 5.27 (s, 2H, CH_2), 4.52 (q, 2H, $J =$ 7 Hz, CH_2O), 1.46 ppm (t, 3H, 7 Hz, CH_3CH_2).

(5-Ethoxycarbonyl-2-pyridylmethyl)bis(2-pyridylmethyl)amine (5-COOEt-TPA):[46] Bis(2-pyridylmethyl)amine in CH_3CN (5 mL) was added dropwise to a suspension of 5-ethoxycarbonyl-2-chloromethylpyridine hydrochloride (1.87 g, 8.4 mmol) and Na_2CO_3 (5.5 g 84 mmol) in CH_3CN (50 mL). The mixture was refluxed for 24 h. After filtering to remove precipitate, the red filtrate was brought to dryness and the residue was purified by column chromatography on activated alumina with EtOAc/hexane (5/2) as eluent.

(5-Dimethylamido-2-pyridylmethyl)bis(2-pyridylmethyl)amine (5-CONMe$_2$-TPA): 5-COOMe-TPA was treated with a 40% aqueous solution of dimethylamine at room temperature for three days. The mixture was extracted with CH_2Cl_2 and the organic layer was collected and dried over $MgSO_4$. Removing the solvent gave the ligand as a red oil. ^{1}H NMR ($CDCl_3$): $\delta = 8.60$ (d, $J = 2$ Hz, H6 of 5-CONMe$_2$-py), 8.54 (d, $J = 4$ Hz, H6 of py), 7.76 (dd, $J = 8$ Hz, 2 Hz, H4 of 5-CONMe$_2$-py), 7.69–7.63 (H3 of 5-CONMe$_2$-py and H4 of py), 7.56 (d, 8 Hz, H3 of py), 7.16 (td, 6 Hz, 1 Hz), 3.93 (s, CH_2 connected to 5-CONMe$_2$-py), 3.91 (s, CH_2 connected to py), 3.12 and 3.01 ppm (both s, N(CH_3)$_2$).

2,4-Diethoxycarbonylpyridine: A solution of 2,4-pyridinedicarboxylic acid (5 g, 30 mmol) and p-toluenesulfonic acid monohydrate (12 g, 63 mmol) in ethanol (300 mL) was refluxed for 24 h. After removing EtOH, $CHCl_3$ followed by saturated aqueous Na_2CO_3 (60 mL) were added and the mixture was extracted with $CHCl_3$ (4 times) and then dried over $MgSO_4$. By removing $CHCl_3$, 2,4-diethoxycarbonylpyridine was obtained as white solid quantitatively. ^{1}H NMR ($CDCl_3$): $\delta = 8.92$ (dd, $J = 5$, 1 Hz, H6-py), 8.65 (dd, $J = 2$, 1 Hz, H3 of py), 8.04 (dd, $J = 5$, 2 Hz, H5 of py), 4.52 (q, 7 Hz, CH_2 of 2-COOEt), 4.46 (q, 7 Hz, CH_2 of 4-COOEt), 1.47 (t, 7 Hz, CH_3 of 2-COOEt), 1.44 ppm (t, 7 Hz, CH_3 of 4-COOEt).

4-Ethoxycarbonyl-2-hydroxymethylpyridine: A solution of $CaCl_2$ (2.50 g, 22.5 mmol) in EtOH at −5 to −10 °C was added dropwise with stirring to a degassed solution of 2,4-diethoxycarbonylpyridine (5.03 g, 22.5 mmol) and $NaBH_4$ (554 mg, 14.6 mmol) in EtOH (200 mL). After completing the addition of $CaCl_2$, the mixture was stirred for 2.5 h at the same temperature and quenched with conc. H_2SO_4. Filtration to remove a white precipitate followed by removal of EtOH by rotary evaporator gave 4-ethoxycarbonyl-2-hydroxymethylpyridine as a pale yellow oil (2.8 g, 69%). ^{1}H NMR ($CDCl_3$): $\delta = 8.71$ (d, 5 Hz, H6 of py), 7.84 (s, H3 of py), 7.77 (d, 5 Hz, H5 of py), 4.85 (s, CH_2OH), 4.42 (q, 7 Hz, CH_2 of Et), 1.42 ppm (t, 7 Hz, CH_3 of Et).

4-Ethoxycarbonyl-2-chloromethylpyridine hydrochloride: A solution of $SOCl_2$ (9.24 g, 77.7 mmol) in $CHCl_3$ (30 mL) was added dropwise to a degassed solution of 4-ethoxycarbonyl-2-hydroxymethylpyridine (15.5 mmol) in $CHCl_3$ (100 mL) at 0 °C with stirring. The mixture was stirred overnight at room temperature and then dried by rotary evaporator to give 4-ethoxycarbonyl-2-chloromethylpyridine hydrochloride as a red solid (3.06 g, 84%). ^{1}H NMR ($CDCl_3$): $\delta = 8.89$ (d, $J = 6$ Hz, H6 of py), 8.41 (s, H3 of py), 8.24 (dd, $J = 6$, 1 Hz, H5 of py), 5.12 (s, CH_2Cl), 4.45 (q, $J = 7$ Hz, CH_2 of 4-COOEt), 1.40 ppm (t, $J = 7$ Hz, CH_3 of COOEt).

Bis(2-pyridylmethyl)(4-ethoxycarbonyl-2-pyridylmethyl)amine (4-COOEt-TPA): Bis(2-pyridylmethyl)amine (2.35 g, 11.8 mmol) was added to a solution of 4-ethoxycarbonyl-2-chloromethylpyridine hydrochloride (3.06 g, 13.0 mmol) and Na_2CO_3 (13.8 g, 0.13 mol) in CH_3CN and the mixture was refluxed for 12 h. After cooling, the mixture was filtered and CH_3CN was removed by rotary evaporator to afford a deep red oil. This crude material was purified on an alumina column eluted with EtOAc/hexane (5/2) to give the ligand as a red oil. ^{1}H NMR ($CDCl_3$): $\delta = 8.64$ (d, 5 Hz, H6 of 4-COOEt-py), 8.49 (d, 5 Hz, H6 of py), 8.06 (s, H3 of 4-COOEt-py), ca. 7.66 (H5 of 4-COOEt-py), 7.62 (td, 5 Hz, 2 Hz, H4 of py), 7.11 (tt, 6 Hz, 1 Hz, H5 of py), 4.38 (q, 7 Hz, CH_2 of Et), 3.93 (s, CH_2 connected to 4-COOEt-py), 3.87 (s, CH_2 connected to py), 1.38 ppm (t, 7 Hz, CH_3 of Et).

Bis(4-ethoxycarbonyl-2-pyridylmethyl)(2-pyridylmethyl)amine (4-(COOEt)$_2$-TPA): 2-Pyridylmethylamine (0.81 g, 7.5 mmol) was added dropwise with stirring to a solution of 4-ethoxycarbonyl-2-chloromethylpyridine hydrochloride (3.88 g, 16.4 mmol) and Na_2CO_3 (17.3 g, 0.16 mol) in CH_3CN and the mixture was refluxed for 13 h. After the same workup as for 4-COOEt-TPA, the mixture was eluted on an alumina column with EtOAc/hexane (5/2) to give the ligand as a red oil. ^{1}H NMR ($CDCl_3$): $\delta = 8.67$ (d, 5 Hz, H6 of 4-COOEt-py), 8.53 (d, 5 Hz, H6 of py), 8.08 (s, H3 of 4-COOEt-py), 7.69 (overlap of H5 of 4-COOEt-py with H4 of py), 7.61 (d, 7 Hz, H3 of py), 7.16 (td, 6 Hz, 1 Hz, H5 of py), 4.41 (q, 7 Hz, CH_2 of Et), 4.01 (s, CH_2 connected to 4-COOEt-py), 3.96 (s, CH_2 connected to py), 1.41 ppm (t, 7 Hz, CH_3 of Et).

Synthesis of Ru^{III} mononuclear complexes was performed by procedures previously reported.[19b] [$RuCl_2$(5-CONMe$_2$-TPA)]ClO_4·H_2O (**3**·H_2O) was purified by quick recrystallization from MeOH, and [$RuCl_2$(4-COOEt-TPA)]ClO_4·H_2O (**4**·H_2O) and [$RuCl_2${4-(COOEt)$_2$-TPA}]ClO_4·H_2O (**5**·H_2O) were purified by quick recrystallization from acetone/2-propanol. **3**·H_2O: elemental analysis (%) calcd for $C_{21}H_{23}N_5OCl_2Ru{\cdot}ClO_4{\cdot}H_2O$: C 38.75, H 3.87, N 10.76; found: C 38.59, H 3.63, N 10.40. **4**· H_2O: elemental analysis (%) calcd for $C_{21}H_{22}N_4O_4Cl_2Ru{\cdot}ClO_4{\cdot}H_2O$: C 38.69, H 3.71, N 8.59; found: C 38.60, H 3.43, N 8.42. **5**·H_2O: elemental analysis (%) calcd for $C_{24}H_{26}N_4O_4Cl_2Ru{\cdot}ClO_4$: C 40.84, H 3.71, N. 7.94; found: C 40.80, H 3.51, N 7.94.

X-ray crystallography on [$RuCl_2$(5-CONMe$_2$-TPA)]ClO_4·$^1/_2$ C_2H_5OH (3·$^1/_2$ C_2H_5OH): A single crystal of this compound was grown from a CH_2Cl_2/EtOH solution and mounted on a glass capillary with Paraton oil. A total of 2482 frames of data were collected on a Siemens SMART CCD area detector system by a narrow-frame method with scan widths of 0.3° in ω and 30 s exposure times at a crystal-to-detector distance of 3.98 cm. Frames were integrated with the Siemens SAINT program.

All refinements were accomplished by using SHELXS-97.[47] Refinement on F^2 was performed for all reflections. The weighted R factor R_w and goodness of fit S are based on F^2, and the conventional R factors R on F, with F set to zero for negative F^2. The threshold expression of $F^2 > 2\sigma(F^2)$ was used only for calculating R factors(gt) etc. and was not relevant to the choice of reflections for refinement. R factors based on F^2 are statistically about twice as large as those based on F, and R factors based on all data are even larger. The three oxygen atoms of the ClO_4^- counterion sit on two sites with occupancies of 0.54(2) and 0.46(2). Since the ethanol molecules were heavily disordered around inversion centers, restraints were applied for the bond lengths. The occupancies are as fol-

 © 2007 Wiley-VCH Verlag GmbH & Co. KGaA, Weinheim

Table 5. Crystallographic data for **2′** and **3**·C_2H_5OH.

	2′	**3**·1/2 C_2H_5OH
formula	$C_{21}H_{24}N_4RuCl_2PF_6$	$C_{22}H_{23}N_5RuCl_3O_{5.50}$
formula weight	649.39	652.87
crystal dimensions [mm]	0.50×0.20×0.20	0.22×0.04×0.02
crystal system	monoclinic	monoclinic
space group	$P2_1/a$ (no. 14)	$P2_1/c$ (no. 14)
a [Å]	13.4834(7)	15.1402(1)
b [Å]	12.5966(5)	11.9799(2)
c [Å]	14.9799(8)	15.5885(2)
β [°]	99.944(4)	112.23(1)
V [Å^3]	2506.0(2)	2617.33(6)
Z	4	4
ρ_{calcd} [g cm^{-3}]	1.721	1.657
$\mu(Mo_{K\alpha})$ [cm^{-1}]	9.65	9.50
T [K]	99	108
reflections measured	6349	41364
observed reflections	3060 ($I>3\sigma(I)$)	5086 ($F^2>2\sigma(F^2)$)
parameters	317	373
R[a], wR[b]	0.028, 0.047	0.062, 0.154
GOF	1.14	1.04

[a] $R=\Sigma||F_o|-|F_c||/\Sigma|F_o|$. [b] $wR=[\Sigma w(F_o^2-F_c^2)^2/\Sigma w(F_o^2)^2]^{1/2}$.

lows: 0.28(2), 0.140(8), and 0.22(2). Crystallographic data are summarized in Table 5.

X-ray crystallography on [$RuCl_2$(5-Me_3-TPA)]PF_6 (2′): A slight excess of NH_4PF_6 in MeOH was added to a hot solution of **2** in MeOH. While cooling the solution to room temperature, red crystals of **2′** formed. Elemental analysis (%) calcd for $C_{21}H_{24}N_4Cl_2RuPF_6$: C 38.84, H 3.73, N 8.63; found: C 38.75, H 3.76, N 8.67. A red crystal was mounted on a glass fiber. All measurements were made on a Rigaku RAXIS-RAPID Imaging Plate diffractometer with graphite-monochromated $Mo_{K\alpha}$ ($\lambda=$ 0.71069 Å) radiation. Indexing was performed from two oscillations which were exposed for 1.7 min. The data were collected at -180 ± 1 °C to a maximum 2θ value of 55.0°. Exposure time was 2.00 min deg^{-1}. Data were processed by the PLUTO-AUTO program package. A symmetry-related absorption correction using the program ABSCOR was applied which resulted in transmission factors ranging from 0.64 to 0.82. The data were corrected for Lorentzian and polarization effects. A correction for secondary extinction was applied. The structure was solved by direct methods and expanded by using Fourier techniques. All non-hydrogen atoms were refined anisotropically and hydrogen atoms were refined isotropically. The atomic scattering factors were taken from ref. [48], and anomalous dispersion effects were included; the values for $\Delta f'$ and $\Delta f''$ were taken from ref. [49]. All calculations were performed with the teXsan crystallographic software package.[50] Crystallographic data are summarized in Table 5.

CCDC-635599 (**2′**) and CCDC-635598 (**3**) contain the supplementary crystallographic data for this paper. These data can be obtained free of charge from the Cambridge Crystallographic Data Centre via www.ccdc.cam.ac.uk/data_request/cif.

Electrochemical measurements: All cyclic voltammograms were recorded on an HECS 312B dc pulse polarograph (Fuso Electrochemical System attached to a HECS 321B potential sweep unit of the same manufacture). A platinum disk (3 mm o.d.) was employed as working electrode, a platinum coil as counterelectrode, and silver/silver nitrate ($Ag/AgNO_3$) electrode as a reference electrode. All measurements were carried out in CH_3CN containing 0.1 M nBu_4NClO_4 as supporting electrolyte under N_2 at ambient temperatures. The redox potentials were determined relative to ferrocene/ferricenium couple as reference (0 V).

Spectroelectrochemistry for 1–5: Acetonitrile solutions of **1–5** were electrolyzed at appropriate potentials on the basis of the redox potentials obtained by cyclic voltammetry in the presence of 0.1 M TBAP under N_2 at room temperature. UV/Vis spectra were recorded on a Shimadzu UV-3100 spectrophotometer with use of a Hokuto Denko HSV-100 Electrochemical Analyzer as a potentiostat.

Catalytic oxygenation of cyclohexane with *m*-chloroperbenzoic acid: Solid *m*-chloroperbenzoic acid (1.0×10^{-3} mol, 0.2 M) was added to a solution (5 mL) of a catalyst (1.0×10^{-5} mol, 2×10^{-3} M) and cyclohexane (1.9 M) in the presence of benzonitrile as an internal standard, which had been degassed by three freeze–pump–thaw cycles. The reaction mixture was stirred at room temperature with bubbling of N_2, which passed through dry CH_3CN prior to introduction. Quantitative product analysis was made by GC measurements. Kinetic isotope effects in cyclohexane oxidation were determined by using a 1:1 mixture of C_6H_{12} and C_6D_{12} as substrate under the same conditions as mentioned above.

Oxidation of adamantane was performed in CH_3CN under N_2 at room temperature. The reaction conditions were the same as those for cyclohexane oxidation except that 100 equiv of adamantine was used as the substrate without bubbling N_2.

$H_2{}^{18}O$ experiments were done by adding 40 μL of $H_2{}^{18}O$ under the conditions described above, and products were analyzed by GC-MS. GC-MS analyses were performed on a Shimadzu GC-17A equipped with a DB-5MS column (Agilient Technologies, 30 m) and a mass spectrograph (Shimadzu QP-5050) as detector.

UV/Vis Spectroscopy on the reaction mixture of 2 and *m*-CPBA in CH_3CN: A solution of *m*CPBA (50 equiv) in CH_3CN was added to a solution of **2** in CH_3CN (0.13 mM) at −30 °C. The UV/Vis spectra were measured in a 1 cm Pyrex glass cell on a Shimadzu UV 3100 PC spectrophotometer equipped with a NESLAB ULT-80-DD cooling system to monitor the reaction.

Resonance Raman spectroscopy: 30 equivalents of *m*CPBA in CH_3CN was added to a solution containing the catalyst (2 mM) and 10 μL of $H_2{}^{16}O$ or $H_2{}^{18}O$ in CH_3CN (0.5 mL) at −30 °C by syringe. Resonance Raman spectra were obtained on a SpectraPro-300i (Acton Research Co.) spectrograph (operating with a 2400-groove grating) using a Spectra-Physics Beamlok 2060 Kr ion laser (413.1 nm) and a Princeton Instruments (LN-1100PB) liquid-N_2-cooled CCD detector in spinning cells (2 cm diameter, 1500 rpm) with a laser power of 20 mW, 90° scattering geometry, and 20 min data accumulation. The temperature was monitored with a thermocouple at the sample point and controlled to be −30 °C by the flow rate of cold nitrogen gas, which flowed through liquid N_2 to a cell in a quartz Dewar vessel. Peak frequencies were calibrated relative to a toluene standard and were accurate to ±1 cm^{-1}. During each Raman experiment, UV/Vis spectra were simultaneously measured on a Hamamatsu PMA-11 CCD spectrometer with photal MC-2530 as light source (D_2/W).

Acknowledgements

This work was supported by Grants-in-Aid from the Ministry of Education, Culture, Sports, Science, and Technology of Japan. We thank Dr. Mikio Yasutake (Kinki University, Fukuoka, Japan) for his help with the X-ray analysis.

[1] R. A. Sheldon, J. K. Kochi, *Metal-Catalyzed Oxidations of Organic Compounds*, Academic Press, New York, **1981**.
[2] A. E. Shilov, G. B. Shul′pin, *Chem. Rev.* **1997**, *97*, 2879–2932.
[3] a) M.-H. Baik, M. Newcomb, R. A. Friesner, S. J. Lippard, *Chem. Rev.* **2003**, *103*, 2385–2419; b) M. Merkx, D. A. Kopp, M. H. Sazinsky, J. L. Blazyk, J. Müller, S. J. Lippard, *Angew. Chem.* **2001**, *113*, 2860–2888; *Angew. Chem. Int. Ed.* **2001**, *40*, 2782–2807; c) L. Que, Jr., R. Y. N. Ho, *Chem. Rev.* **1996**, *96*, 2607–2624; d) B. J. Wallar, J. D. Lipscomb, *Chem. Rev.* **1996**, *96*, 2625–2657.
[4] C. A. Tolman, J. D. Druliner, M. J. Nappa, N. Herron in *Activation and Functionalization of Alkanes* (Ed.: C. L. Hill), Wiley, New York, **1989**, pp. 303–360.
[5] a) B. Meunier, *Chem. Rev.* **1992**, *92*, 1411–1456; b) M. J. Gunter, P. Turner, *Coord. Chem. Rev.* **1991**, *108*, 115–161; c) D. Dolphin, T. G. Traylor, L. Y. Xie, *Acc. Chem. Res.* **1997**, *30*, 251–259.

 © 2007 Wiley-VCH Verlag GmbH & Co. KGaA, Weinheim

[6] a) M. Costas, K. Chen, L. Que, Jr., *Coord. Chem. Rev.* **2000**, *200–202*, 517–544; b) M. P. Jensen, M. Costas, R. Y. N. Ho, J. Kaizer, A. Mariata i Payeras, E. Münck, L. Que, Jr., J.-U. Rohde, A. Stubna, *J. Am. Chem. Soc.* **2005**, *127*, 10512–10525.
[7] a) H.-F. Hsu, Y. Dong, L. Shu, V. Young, Jr., L. Que, Jr., *J. Am. Chem. Soc.* **1999**, *121*, 5230–5237; b) H. Miyake, K. Chen, S. J. Lange, L. Que, Jr., *Inorg. Chem.* **2001**, *40*, 3534–3538; c) M. H. Lim, J.-U. Rohde, A. Stubna, M. R. Bukowski, M. Costas, R. Y. N. Ho, E. Münck, W. Nam, L. Que, Jr., *Proc. Natl. Acad. Sci., USA* **2003**, 100, 3665–3670.
[8] a) R. A. Leising, J. Kim. M. Pérez, L. Que, Jr., *J. Am. Chem. Soc.* **1993**, *115*, 9524–9530; b) T. Kojima, R. A. Leising, S. Yan, L. Que, Jr., *J. Am. Chem. Soc.* **1993**, *115*, 11328–11335.
[9] a) M. Fujita, M. Costas, L. Que, Jr., *J. Am. Chem. Soc.* **2003**, *125*, 9912–9913; b) K. Chen, L. Que, Jr., *Angew. Chem.* **1999**, *111*, 2365–2368; *Angew. Chem. Int. Ed.* **1999**, *38*, 2227–2229.
[10] a) Y. Zang, J. Kim, Y. Dong, E. C. Wilkinson, E. H. Appleman, L. Que, Jr., *J. Am. Chem. Soc.* **1997**, *119*, 4197–4205; b) K. Chen, L. Que, Jr., *Chem. Commun.* **1999**, 1375–1376.
[11] W.-P. Yip, W.-Y. Yu, N. Zhu, C.-M. Che, *J. Am. Chem. Soc.* **2005**, *127*, 14239–14249.
[12] a) H. Ohtake, T. Higuchi, M. Hirobe, *J. Am. Chem. Soc.* **1992**, *114*, 10660–10662; b) C. Ho, W.-H. Leung, C.-M. Che, *J. Chem. Soc. Dalton Trans.* **1991**, 2933–2939.
[13] a) R. A. Leising, K. J. Takeuchi, *Inorg. Chem.* **1987**, *26*, 4391–4393; b) M. E. Marmion, K. J. Takeuchi, *J. Am. Chem. Soc.* **1986**, *108*, 510–511.
[14] a) A. M. Khenkin, L. J. W. Shimon, R. Neumann, *Inorg. Chem.* **2003**, *42*, 3331–3339; b) R. Neumann, M. Dahan, *J. Am. Chem. Soc.* **1998**, *120*, 11969–11976; c) R. Neumann, M. Dahan, *Nature* **1997**, *388*, 353–355. See also: Y. Cindy-Xing, R. G. Finke, *Inorg. Chem.* **2005**, *44*, 4175–4188.
[15] For 2,2′-bipyridines, see: T. C. Lau, C. M. Che, W.-O. Lee, C.-K. Poon, *J. Chem. Soc. Chem. Commun.* **1988**, 1406–1407. For 1,10-phenanthrolines, see: a) A. S. Goldstein, R. H. Beer, R. S. Drago, *J. Am. Chem. Soc.* **1994**, *116*, 2424–2429; b) A. S. Goldstein, R. S. Drago, *J. Chem. Soc. Chem. Commun.* **1991**, 21–22.
[16] C.-M. Che, V. W.-W. Yam, T. C. W. Mak, *J. Am. Chem. Soc.* **1990**, *112*, 2284–2291.
[17] C.-M. Che, W.-T. Tang, W.-T. Wong, T.-F. Lai, *J. Am. Chem. Soc.* **1989**, *111*, 9048–9056.
[18] a) T. Kojima, *Chem. Lett.* **1996**, 121–122; b) M. Yamaguchi, H. Kousaka, T. Yamagishi, *Chem. Lett.* **1997**, 769–770; c) K. Jitsukawa, Y. Oka, S. Yamaguchi, H. Masuda, *Inorg. Chem.* **2004**, *43*, 8119–8129; d) M. Yamaguchi, H. Kousaka, S. Izawa, Y. Ichii, T. Kumano, D. Masui, T. Yamagishi, *Inorg. Chem.* **2006**, *45*, 8342–8354.
[19] a) M. Palucki, N. S. Finney, P. J. Pospisil, M. L. Güler, T. Ishida, E. N. Jacobsen, *J. Am. Chem. Soc.* **1998**, *120*, 948–954; b) E. N. Jacobsen, W. Zhang, M. L. Güler, *J. Am. Chem. Soc.* **1991**, *113*, 6703–6704.
[20] a) T. Kojima, T. Amano, Y. Ishii, M. Ohba, Y. Okaue, Y. Matsuda, *Inorg. Chem.* **1998**, *37*, 4076–4085; b) T. Kojima, K. Hayashi, Y. Matsuda, *Chem. Lett.* **2000**, 1008–1009; c) T. Kojima, Y. Matsuda, *J. Chem. Soc. Dalton Trans.* **2001**, 958–960; d) T. Kojima, T. Sakamoto, Y. Matsuda, K. Ohkubo, S. Fukuzumi, *Angew. Chem.* **2003**, *115*, 5101–5104; *Angew. Chem. Int. Ed.* **2003**, *42*, 4951–4954; e) T. Kojima, T. Sakamoto, T. Matsuda, *Inorg. Chem.*, **2004**, *43*, 2243–2245; f) T. Kojima, K. Hayashi, Y. Matsuda, *Inorg. Chem.* **2004**, *43*, 6793–6804; g) T. Kojima, S. Miyazaki, K. Hayashi, Y. Shimazaki, F. Tani, Y. Naruta, Y. Matsuda, *Chem. Eur. J.* **2004**, *10*, 6402–6410; h) T. Kojima, Y. Matsuda, *Chem. Lett.* **2005**, *34*, 258–259; i) T. Kojima, K. Hayashi, Y. Shiota, Y. Tachi, Y. Naruta, T. Suzuki, K. Uezu, K. Yoshizawa, *Bull. Chem. Soc. Jpn.* **2005**, *78*, 2152–2158; j) S. Miyazaki, K. Ohkubo, T. Kojima, S. Fukuzumi, *Angew. Chem.* **2007**, *119*, 923–926; *Angew. Chem. Int. Ed.* **2007**, *46*, 905–908.
[21] a) T. Kojima, H. Matsuo, Y. Matsuda, *Inorg. Chim. Acta* **2000**, *300–302*, 661–667; b) T. Kojima in *Electronic Encyclopedia of Reagents for Organic Synthesis*, Wiley, **2005**, DOI: 10.1002/047084289X.rn00597.
[22] T. Kojima, Y. Matsuda, *Chem. Lett.* **1999**, 81–82.
[23] F. Bigoli, A. Braibanti, M. A. Pelinghelli, A. Tiripicchio, *Acta Crystallogr. Sect. B* **1972**, *28*, 962.
[24] Z. Tyeklár, R. R. Jacobson, N. Wei, N. N. Murthy, J. Zubieta, K. D. Karlin, *J. Am. Chem. Soc.* **1993**, *115*, 2677–2689.
[25] C. M. Elliott, J. K. Arnette, R. R. Krebs, *J. Am. Chem. Soc.* **1985**, *107*, 4904–4911.
[26] The values were taken from H. H. Jaffé, *Chem. Rev.* **1953**, *53*, 191–261. The σ value of $CONH_2$ (*meta*) was used for 5-$CONMe_2$-TPA.
[27] J. T. Groves, Z. Gross, M. K. Stern, *Inorg. Chem.* **1994**, *33*, 5065–5072.
[28] K. M. Kadish, *Prog. Inorg. Chem.* **1986**, *34*, 435–605.
[29] M. Palucki, N. S. Finney, P. J. Pospisil, M. L. Güler, T. Ishida, E. N. Jacobsen, *J. Am. Chem. Soc.* **1998**, *120*, 948–954.
[30] V. Skarda, M. J. Coon, A. P. Lewis, G. S. G. McAuliffe, A. J. Thomson, D. J. Robbins, *J. Chem. Soc. Perkin Trans. 2* **1984**, 1309–1311.
[31] T. Kojima, H. Matsuo, Y. Matsuda, *Chem. Lett.* **1998**,1085–1086.
[32] L. M. Slaughter, J. P. Collman, T. A. Eberspacher, J. I. Brauman, *Inorg. Chem.* **2004**, *43*, 5198–5204.
[33] Reaction conditions were the same as described in the Experimental Section except that cyclohexanol was used as substrate. We also conducted a competitive reaction with an equimolar mixture of cyclohexanol and cyclooctane as substrate and observed formation of cyclohexanone as major product and a small amount of cyclooctanol under the same conditions.
[34] A. A. Fokin, P. R. Schreiner, *Chem. Rev.* **2002**, *102*, 1551–1593.
[35] M. K. Seo, J.-H. In, S. O. Kim, N. Y. Oh, J. Hong, J. Kim, L. Que, Jr. W. Nam, *Angew. Chem.* **2004**, *116*, 2471–2474; *Angew. Chem. Int. Ed.* **2004**, *43*, 2417–2420.
[36] The chlorophenyl radical may also abstract a hydrogen atom from *m*CPBA to produce *m*CPB$^{\bullet}$, accompanied by generation of a *m*CBA$^{\bullet}$ radical that undergoes decarboxylation to regenerate the chlorophenyl radical. For such radical-chain decomposition of hydroperoxides, see: S. Fukuzumi, Y. Ono, *J. Chem. Soc. Perkin Trans. 2* **1977**, 625–630.
[37] a) W. Nam, J. S. Valentine, *J. Am. Chem. Soc.* **1993**, *115*, 1772–1778; b) K. A. Lee, W. Nam, *J. Am. Chem. Soc.* **1997**, *119*, 1916–1922; c) W. Nam, I. Kim, M. H. Lim, H. J. Choi, J. S. Lee, H. G. Jang, *Chem. Eur. J.* **2002**, *8*, 2067–2071; d) W. J. Song, Y. J. Sun, S. K. Choi, W. Nam, *Chem. Eur. J.* **2006**, *12*, 130–137.
[38] J. A. Kerr, *Chem. Rev.* **1966**, *66*, 465–500.
[39] A. Bravo, H.-R. Bjorsvik, F. Fontana, F. Minisi, A. Serri, *J. Org. Chem.* **1996**, *61*, 9409–9416.
[40] H. Yamada, T. Koike, J. K. Hurst, *J. Am. Chem. Soc.* **2001**, *123*, 12775–12780.
[41] I. R. Paeng, K. Nakamoto, *J. Am. Chem. Soc.* **1990**, *112*, 3289–3297.
[42] B. Giese in *Houben-Weyl, Methoden der Organischen Chemie, Band E 19a, C-Radikale* (Eds.: M. Regitz, B. Giese) Thieme, Stuttgart, New York, **1989**, p. 140.
[43] a) K. Jitsukawa, Y. Oka, S. Yamaguchi, H. Masuda, *Inorg. Chem.* **2004**, *43*, 8119–8129; b) K. Jitsukawa, H. Shiozaki, H. Masuda, *Tetrahedron Lett.* **2002**, *43*, 1491–1494.
[44] a) G. Anderegg, F. Wenk, *Helv. Chim. Acta* **1967**, *50*, 2330–2332; b) B. G. Gafford, R. A. Holewelda, *Inorg. Chem.* **1989**, *28*, 60–66.
[45] Y. Dong, H. Fujii, M. P. Hendrich, R. A. Leising, G. Pan, C. R. Randall, E. C. Wilkinson, Y. Zang, L. Que Jr. , B. G. Fox, K. Kauffmann, E. Münck, *J. Am. Chem. Soc.* **1995**, *117*, 2778–2792.
[46] T. Sasaki, N. Nakamura, Y. Naruta, *Chem. Lett.* **1998**, 351–352.
[47] G. M. Sheldrick, SHELXS-97, A software package for the solution and refinement of X-ray data, University of Göttingen, Göttingen, Germany.
[48] *International Tables for X-Ray Crystallography, Vol. IV*, Kynoch Press, Birmingham, England, **1974**.
[49] *International Tables for X-Ray Crystallography, Vol. C*, Kluwer Academic Publishers, Boston, MA, **1992**.
[50] teXsan: Crystal Structure Analysis Package, Molecular Structure Corporation, **1985** and **1999**.

Received: February 3, 2007
Published online: July 12, 2007

 © 2007 Wiley-VCH Verlag GmbH & Co. KGaA, Weinheim